European Journal of Nuclear Medicine and Molecular Imaging (2022) 49:2877–2888
https://doi.org/10.1007/s00259-022-05729-5

ORIGINAL ARTICLE

Comparison of the diagnostic efficacy of ^{68} Ga-FAPI-04 PET/MR and ^{18}F-FDG PET/CT in patients with pancreatic cancer

Zeyu Zhang[1] · Guorong Jia[1] · Guixia Pan[1] · Kai Cao[2] · Qinqin Yang[1] · Hongyu Meng[3] · Jian Yang[1] · Lu Zhang[1] · Tao Wang[1] · Chao Cheng[1] · Changjing Zuo[1]

Received: 19 September 2021 / Accepted: 13 February 2022 / Published online: 4 March 2022

Abstract

Purpose We sought to assess the performance of ^{68} Ga-FAPI-04 PET/MR for the diagnosis of primary tumours as well as metastatic lesions in patients with pancreatic cancer and to compare the results with those of ^{18}F-FDG PET/CT.

Methods Prospectively, we evaluated 33 patients suspected to have pancreatic adenocarcinoma, of whom thirty-two were confirmed by histopathology, and one had autoimmune pancreatitis confirmed by needle biopsy and glucocorticoid treatment. Within 1 week, each patient underwent both ^{68} Ga-FAPI-04 PET/MR and ^{18}F-FDG PET/CT. Comparisons of the detection abilities for primary tumours, lymph nodes, and metastases were conducted for the two imaging approaches. The original maximum standard uptake values (SUV_{max}) and normalised SUV_{max} (SUV_{max}/SUV_{bkgd}) of paired lesions on ^{68} Ga-FAPI-04 PET/MR and ^{18}F-FDG PET/CT were measured and compared.

Results Thirty pancreatic cancer patients and three pancreatitis patients were enrolled. ^{68} Ga-FAPI-04 PET/MR and ^{18}F-FDG PET/CT exhibited equivalent (100%) detection rates for primary tumours. The original/normalised SUV_{max} of primary tumours on ^{68} Ga-FAPI-04 PET was markedly higher than that on ^{18}F-FDG ($p < 0.05$). Sixteen pancreatic cancer patients had pancreatic parenchymal uptake, whereas ^{18}F-FDG PET images showed parenchymal uptake in only four patients (53.33% vs. 13.33%, $p < 0.001$). ^{68} Ga-FAPI-04 PET detected more positive lymph nodes than ^{18}F-FDG PET (42 vs. 30, $p < 0.001$), while ^{18}F-FDG PET was able to detect more liver metastases than ^{68} Ga-FAPI-04 (181 vs. 104, $p < 0.001$). In addition, multisequence MR imaging helped explain ten pancreatic cancers that could not be definitively revealed due to ^{68} Ga-FAPI-04 inflammatory uptake and identified more liver metastases than ^{18}F-FDG (256 vs. 181, $p < 0.001$).

Conclusion ^{68} Ga-FAPI-04 PET might be better than ^{18}F-FDG PET in the detection of suspicious lymph node metastases. MR multiple sequence imaging of ^{68} Ga-FAPI-04 PET/MR was helpful for explaining pancreatic lesions in patients with obstructive inflammation and detecting tiny liver metastases.

Keywords ^{68} Ga-FAPI-04 · ^{18}F-FDG · PET/MR · PET/CT · Pancreatic cancer

Zeyu Zhang and Guorong Jia contributed equally.

This article is part of the Topical Collection on Oncology - Digestive tract

✉ Chao Cheng
13501925757@163.com

✉ Changjing Zuo
changjing.zuo@qq.com

[1] Department of Nuclear Medicine, Changhai Hospital, Naval Medical University, 168 Changhai Road, Shanghai 200433, China

[2] Department of Radiology, Changhai Hospital, Naval Medical University, Shanghai 200433, China

[3] Department of Radiology, Shanghai Fourth People's Hospital Affiliated to Tongji University, School of Medicine, Shanghai 200434, China

Introduction

Pancreatic cancer is a malignancy with high mortality. Its global incidence has tripled since the 1950s, ranking as the fourth leading cause of tumour-associated mortalities [1]. Surgical therapy remains the only pancreatic cancer cure. With insidious clinical symptoms, most pancreatic tumours are found at the late stage, resulting in only 10–20% of patients being eligible for surgical resection when detected [2]. Thus, an early pancreatic cancer diagnosis will inform the choice of optimal therapy. Currently, relative to conventional imaging examinations (computed tomography (CT) and magnetic resonance imaging (MRI)), positron emission tomography (PET) with ^{18}F-fluorodeoxyglucose (FDG) has higher sensitivity

and specificity for pancreatic cancer staging [3]. Therapeutic responses and disease recurrence for pancreatic cancer have also been evaluated by ^{18}F-FDG PET/CT [4]. Furthermore, ^{18}F-FDG PET/CT imaging parameters may predict its treatment efficacy and clinical outcome [5]. It should be noted that ^{18}F-FDG sometimes produces false positives for various nonmalignant lesions exhibiting moderate FDG avidity (e.g. reactive lymph nodes or inflammation), and produces false negatives in about 10% of pancreatic cancer patients [6].

Pancreatic cancer is characterised by a prominent desmoplastic reaction. The desmoplastic stroma is produced by mainly pancreatic stellate cells (PSCs) [7]. Cancer-associated fibroblasts (CAFs) are partly derived from PSCs and transform their tumour-promoting biological properties by a cross talk with neoplastic cells [8, 9]. CAFs promote the proliferation and growth of pancreatic cancer cells and thus contribute to the progression, invasion, metastasis, and therapy resistance [10, 11]. Unlike normal fibroblasts, CAFs express specific marker fibroblast activation protein (FAP) on their surface [12, 13]. Based on FAP-specific inhibitors (FAPI), radiopharmaceuticals targeting FAP have been developed. ^{68} Ga-labelled FAPI (^{68} Ga-FAPI-04) has been recently introduced as a promising tumour imaging agent targeting CAFs. High uptake of radioactive FAPI has been confirmed in various malignant cancers, including pancreatic cancer [14–16]. Röhrich et al. found that relative to contrast-enhanced CT (CECT), ^{68} Ga-FAPI-04 PET/CT is better at detecting recurrent and metastatic lesions in patients with pancreatic ductal carcinoma (PDAC) [16].

It is well known that the low resolution of low-dose CT does not allow satisfactory anatomic evaluation of lesions in soft tissue. The combination of PET and MRI is a very capable hybrid imaging technique that integrates the superiority of MRI soft-tissue contrast with the molecular specificity and sensitivity of PET [17]. Integrated PET/MR, as a versatile modality, can potentially compensate for the known limitation of PET/CT in detecting small pancreatic cancer, distinguishing mimics, and detecting small hepatic metastases [6, 18].

This is a prospective study to determine if the performance of ^{68} Ga-FAPI-04 PET/MR is superior to that of ^{18}F-FDG PET/CT in diagnosing primary tumours, involvement of the lymph nodes, and distant metastases in patients with pancreatic cancer and to compare the potential impacts of both on therapeutic management.

Materials and methods

Patients

This prospective study was permitted by the Ethical Committee of the First Affiliated Hospital of Naval Medical University (Changhai Hospital, CHEC2020-071). All patients signed an informed consent form prior to participation. Inclusion criteria were as follows: (i) patients with clinical symptoms or blood tumour marker abnormalities were suspected of pancreatic adenocarcinoma by radiologic examinations (CECT or MRI); (ii) patients willing to accept both ^{68} Ga-FAPI-04 PET/MR and ^{18}F-FDG PET/CT scans; (iii) patients were subjected to both ^{68} Ga-FAPI-04 PET/MR as well as ^{18}F-FDG PET/CT scans within 1 week; (iv) no contraindications to MRI. The exclusion criteria were as follows: (i) pregnancy; (ii) subjected to invasive examinations prior to PET scans, including histopathological biopsy, endoscopic retrograde cholangiopancreatography (ERCP), and stent placement; (iii) received radiotherapy or chemotherapy before PET scans; (iv) no available complete clinical or pathological records; (v) exclusion of typical cystic or blood-rich pancreatic tumours (e.g. solid pseudopapillary neoplasm of the pancreas, pancreatic neuroendocrine neoplasms, etc.); (vi) inability or unwillingness of the research participant, parent, or legal representative to provide written informed consent.

Biological and clinical data, including sex, clinical presentation, age, and laboratory indices, were collected from each patient. The final diagnosis was based on the histopathological assessments of tumour samples harvested by surgical resection or biopsy. For patients for whom tissue diagnosis is not appropriate, radiological follow-up is required. The minimum follow-up time was 3 months.

Radiopharmaceuticals

The synthesis and labelling of ^{68} Ga-FAPI-04 were performed according to a previously documented method [19]. ^{68} Ga was obtained from an in-house ^{68}Ge-to-^{68} Ga generator (ITG, Germany). Chelation was performed after adjusting the pH using sodium acetate. Then, for 10 min, heating of the reaction mixture was performed at 100 °C. The reaction integrity was assessed by radio-liquid chromatography. Solid-phase extraction of ^{68} Ga compounds was performed before injection. The final product was sterile and pyrogen-free, and the radiochemical purity was > 95%.

^{18}F-FDG injections were obtained from Shanghai Atom Kexing Pharmaceutical Co., Ltd. (their radiochemical purity was > 95%).

^{68} Ga-FAPI-04 PET/MR imaging

PET/MR assessments were conducted on an integrated PET/MR scanner (Biograph mMR; Siemens Healthcare, Erlangen, Germany) that has a combination of PET and 3.0-T MRI scanners. The intravenous injection activity of ^{68} Ga-FAPI-04 was 1.85–3.70 MBq/kg. After a fast and simple MRI scout imaging sequence, a PET scan (3 min/bed

position) was conducted for the whole body from the skull vertex to mid-thigh in 5–6 bed positions. MRI was concurrently conducted using the protocol: T1-weighted 3D volumetric interpolated breath-hold examination (VIBE) with Dixon fat saturation (T1-VIBE-DIXON) (3D, transversal, TR 4.07 ms, TE 1.28 ms, flip angle 12°, 72 slices, 3-mm slice thickness, the field of view (FOV) 400 × 400, voxel size 1.3 × 1.3 × 3.0 mm^3), T2W-BLADE (transversal, TR 3000 ms, TE 89 ms, flip angle 90°, 33 slices, slice thickness 6 mm, FOV 400 × 400, voxel size 1.3 × 1.3 × 6.0 mm^3), DWI (2D, transversal, TR 6270 ms, TE 50 ms, 33 slices, 6-mm slice thickness, FOV 400 × 400, voxel size 1.6 × 1.6 × 6.0 mm^3, *b*-values 50, 800 s/mm^2). The PET data were reconstructed using high-definition PET (HD-PET) (3 iterations, 21 subsets; matrix 172 × 172, voxel size 2.3 × 2.3 × 5.0 mm^3). The Dixon sequence was used to derive MRI-based attenuation correction.

^{18}F-FDG PET/CT imaging

Prior to the ^{18}F-FDG PET/CT scan, study participants were asked to fast for at least 6 h, ensuring a blood glucose (BG) less than 11.1 mmol/L, and then they were intravenously administered ^{18}F-FDG (3.70–5.55 MBq/kg). All acquisitions were performed on a Biograph 64 PET/CT scanner (Siemens Healthcare, Erlangen, Germany) 45–60 min after ^{18}F-FDG injection. The whole-body CT scanning parameters were set as follows: current (170 mA), voltage (120 kV), and scan layer thickness (3 mm). The PET scan was performed after CT scan acquisition and conducted in 5–6 bed positions. Immediately after CT image acquisition, PET data were acquired for 3 min per bed position. Reconstruction of the acquired data was performed by the postprocessing workstation with an iterative TrueD reconstruction system (Siemens Medical Solutions). Correction attenuation was performed by CT images.

Image interpretation

All reconstructed ^{68} Ga-FAPI-04 PET/MR and ^{18}F-FDG PET/CT images were evaluated using Syngo. Via (Siemens Healthcare, Erlangen, Germany) by two groups of experienced nuclear medicine physicians independently. Any discrepancies were discussed to reach a consensus.

Due to the presence of obstructive inflammation, we assessed the readability of PET uptake in primary lesions. Tumours that could not be accurately localised/discerned on PET images were defined as PET negative; otherwise, they were defined as PET positive. Additionally, the number of primary foci and metastases detected by ^{68} Ga-FAPI-04 or ^{18}F-FDG PET, ^{68} Ga-FAPI-04 PET/MR, and ^{18}F-FDG PET/CT were recorded, and the evaluations were conducted without any information from the other PET scan. The patient's previous CECT/MR images were also referenced during the segmentation.

In this study, if ^{68} Ga-FAPI-04 or ^{18}F-FDG uptake in the lymph node surpassed that in the surrounding tissue, it was considered a positive lymph node. Distant metastases were assessed by abnormal tracer uptake as well as CT or MR imaging findings. Locations and other information on metastases were documented.

To calculate the standard uptake values, circular regions of interest were drawn around the lesions and automatically adapted to a tridimensional volume of interest. For every lesion, the maximum standard uptake value (SUV_{max}) was automatically calculated by the syngo. via software. To ensure that the SUV_{max} was relatively comparable, referring to Qin et al. [20], the original SUV_{max} was normalised using the following formula: $NormalisedSUVmax = OriginalSUVmax/SUVbkgd$. SUV_{bkgd} refers to the average SUV of the background tissue. We normalised the average SUV of the descending aorta, liver, and spleen to the original SUV_{max}.

If there were fewer than five lesions in a single organ/region, all lesions were quantitatively assessed. If there were more than five lesions in a single organ/region, the five lesions with the highest activity were quantitatively evaluated.

Statistical analysis

Data analyses were conducted using SPSS (version 26.0; IBM, Armonk, NY, USA). The quantitative data are presented as the mean ± SD. The chi-squared test was used to compare the number of positive lesions identified by two examinations. We used a paired *t* test to compare different paired ^{18}F-FDG and ^{68} Ga-FAPI-04 PET SUV_{max}. $p < 0.05$ was the cutoff for significance, and all tests were two-sided.

Results

Patient characteristics

We recruited 33 patients between January 2020 and August 2021. Patient information, including clinical presentation and laboratory indices, was recorded, as summarised in Table 1. The median time interval between the two scans was 2 days (range: 1–6 days); see Supplementary Table 1 for further details.

Clinical diagnosis of suspicious patients

Among the 33 patients, 30 cases were confirmed as pancreatic cancer by histopathological results, with nine patients undergoing surgical resection and 21 patients undergoing

endoscopic ultrasound-fine needle aspiration (EUS-FNA) (Supplementary Table 1). Of the nine surgical samples, eight were duct adenocarcinoma, and one was adenosquamous carcinoma.

Table 1 Clinical characteristics of all patients

	Pancreatic cancer ($n=30$)	Pancreatitis ($n=3$)
Population		
Age (range, mean)	48–81, 68.61	47–52, 49.33
Gender (M:F)	17:13	2:1
Laboratory		
CA19-9 (> 37U/ml)	22 (73.33%)	1 (33.33%)
CEA (> 5 ng/ml)	11 (36.67%)	2 (66.67)
History		
Smoking	9 (30.00%)	1 (33.33%)
Alcohol	8 (26.67%)	1 (33.33%)
Diabetes	6 (20.00%)	1 (33.33%)
Hypertension	16 (53.33%)	0
Abdominal pain	24 (80.00%)	1 (33.33%)
Jaundice	4 (13.33%)	1 (33.33%)
Weight loss	15 (50.00%)	1 (33.33%)
Histopathology		
Surgical resection	9 (30.00%)	2 (66.67%)
EUS-FNA	21 (70.00%)	1 (33.33%)

Abbreviations: *CA19-9*, carbohydrate antigen 19–9; *CEA*, carcinoembryonic antigen; *EUS-FNA*, endoscopic ultrasound-fine needle aspiration

The other three patients were confirmed to have pancreatitis. Two patients (patients 31 and 32) were confirmed to have chronic pancreatitis by surgery. In the other patient (patient 33), tumour cells were not detected by needle biopsy, and her clinical symptoms improved after glucocorticoid treatment. The diagnosis of autoimmune pancreatitis was established.

Primary tumour detection

^{68} Ga-FAPI-04 PET/MR and ^{18}F-FDG PET/CT exhibited comparable detection abilities for primary pancreatic tumours with a 100% positive detection rate. Table 2 shows the comparison of uptake parameters (including the original and normalised SUV_{max}) between ^{68} Ga-FAPI-04 and ^{18}F-FDG. Both the original and normalised SUV_{max} of the primary tumour on ^{68} Ga-FAPI-04 PET were higher than those on ^{18}F-FDG ($p<0.05$).

Elevated tracer uptake was observed in the adjacent tissue of the pancreas at the same time in ^{68} Ga-FAPI-04 imaging in 16 patients (53.33%), which masked the tumour uptake in 11 patients (Fig. 1). Density differences were not observed in 12 lesions (75.00%) on low-dose CT images, while all patients (100.0%) showed abnormal signals on multiparameter MR, which enhanced confidence in the interpretation of pancreatic tumours (Table 3). In ^{68} Ga-FAPI-04 PET, there was no significant difference in SUV_{max} between obstructive pancreatic inflammation and pancreatic cancer lesions (SUV_{max}, 13.70 ± 5.15 vs. 12.58 ± 4.44, $p=0.596$). Two of

Table 2 Comparison of the primary tumour, lymph node, and liver metastases between ^{68} Ga-FAPI-04 PET/MR and ^{18}F-FDG PET/CT

		Primary tumour	Lymph nodes	Liver metastases
Lesion number	^{68} Ga-FAPI-04 PET	20	42	104
	^{18}F-FDG PET	30	30	181
	p value	0.001	< 0.001	< 0.001
	^{68} Ga-FAPI-04 PET/MR	30	43	256
	^{18}F-FDG PET/CT	30	30	181
	p value	-	< 0.001	< 0.001
Original SUV_{max}	Paired lesions	30	23	22
	^{68} Ga-FAPI-04 PET	12.58 ± 4.44	9.35 ± 5.42	5.97 ± 2.19
	^{18}F-FDG PET	8.78 ± 3.80	7.77 ± 4.18	8.64 ± 2.04
	p value	0.002	0.648	0.001
Normalised SUV_A	^{68} Ga-FAPI-04 PET	7.26 ± 3.01	5.18 ± 2.85	3.46 ± 1.01
	^{18}F-FDG PET	5.16 ± 4.32	5.39 ± 3.74	6.37 ± 2.56
	p value	0.012	0.330	0.001
Normalised SUV_L	^{68} Ga-FAPI-04 PET	4.54 ± 2.39	4.94 ± 2.93	3.16 ± 0.85
	^{18}F-FDG PET	3.11 ± 1.45	3.44 ± 1.86	4.35 ± 1.72
	p value	0.002	0.101	0.019
Normalised SUV_S	^{68} Ga-FAPI-04 PET	6.30 ± 2.59	4.74 ± 2.53	2.95 ± 0.80
	^{18}F-FDG PET	4.05 ± 1.66	4.31 ± 2.53	4.98 ± 1.35
	p value	< 0.001	0.903	< 0.001

Abbreviations: *A*, descending aorta; *L*, liver; *S*, spleen; "-" means no need to compare

the 16 patients had a clinical history of chronic pancreatitis, and thirteen showed dilated pancreatic ducts on MR or CT images. Diffuse or focal parenchymal uptake in ^{18}F-FDG PET imaging was observed in only four patients (13.33% vs. 53.33%, $p < 0.001$), and the radiographic follow-up data of these four patients were presented in Supplementary Fig. 1. Typical cases are presented in Figs. 2 and 3.

Lymph node assessment

In this study, each lymph node with obvious ^{68} Ga-FAPI-04 or ^{18}F-FDG uptake was deemed a positive lymph node. Among the 15 patients with alleged metastasis of lymph nodes, 33.33% (5/15) showed more positive lymph nodes on ^{68} Ga-FAPI-04 than on ^{18}F-FDG PET. Altogether, 42 and 30 positive lymph nodes were depicted by ^{68} Ga-FAPI-04 and ^{18}F-FDG PET, respectively ($p < 0.001$). In all, compared with ^{18}F-FDG PET, ^{68} Ga-FAPI-04 led to N upstaging in 26.67% (4/15) of patients, and upstaging from N0 to N1 (patient 18) and N0 to N2 (patient 8) occurred in one case. Two patients were upstaged from N1 to N2 (patients 3 and 26). Notably, one ^{18}F-FDG-positive metastatic lymph node was missed by ^{68} Ga-FAPI-04 PET in a patient (patient 28); however, abnormal signals on multiparametric MR of PET/MR enhanced interpretation confidence. Follow-up CT imaging 3 months after chemotherapy revealed shrinkage of the lymph node. Typical cases are presented in Figs. 4 and 5.

There was no significant difference in the uptake of ^{18}F-FDG and ^{68} Ga-FAPI-04 between all 23 double-positive lymph nodes, and the normalised indicators did not affect the results ($p > 0.05$).

Liver metastases

Biopsy of at least one lesion in the liver should be performed in patients with liver metastasis, but it was not mandatory. Of the five patients (patients 8, 9, 26, 29, and 30) with liver metastases (Supplementary Fig. 2), ^{18}F-FDG PET showed more metastatic lesions than ^{68} Ga-FAPI-04 (181 vs. 104, $p < 0.001$). ^{18}F-FDG exhibited a higher uptake than ^{68} Ga-FAPI-04 (SUV_{max}, 8.64 ± 2.04 vs. 5.97 ± 2.19, $p = 0.001$) in all 22 double-positive intrahepatic metastasis lesions, and the normalised indicators did not affect the results. In these five patients, the visual analysis revealed that larger intrahepatic metastases often showed ring-shaped ^{68} Ga-FAPI-04 uptake with tracers around merely the edge of the lesions, and the uptake intensity was significantly lower than that of ^{18}F-FDG. Typical cases are presented in Fig. 6.

All intrahepatic metastases with increased ^{18}F-FDG or ^{68} Ga-FAPI-04 uptake were detected by PET/MR MRI, and more micrometastases were detected by MRI (Table 2).

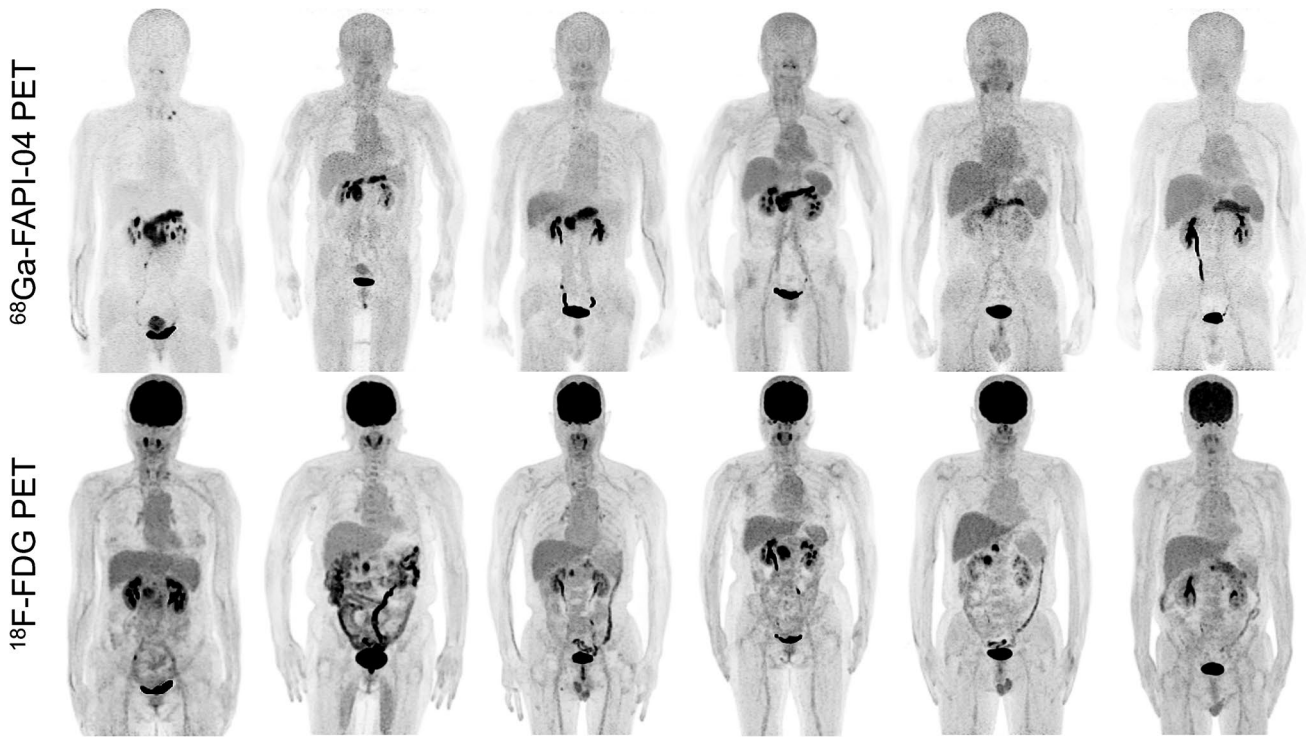

Fig. 1 Representative maximum intensity project (MIP) images of ^{68} Ga-FAPI-04 PET and ^{18}F-FDG PET in patients with concomitant pancreatic obstructive inflammation (patient 3, 14, 17, 19, 24, and 28)

Table 3 Patients with concomitant obstructive inflammation

Patient no	^{68} Ga-FAPI-04 PET		^{18}F-FDG PET		CT density[3]	MRI signal[3]	Pancreatic duct[4]
	Inflammation[1]	Boundary[2]	Inflammation[1]	Boundary[2]			
1	+	−	−	−	−	+	−
2	+	+	−	−	−	+	+
3	+	+	−	−	+	+	+
6	+	+	+	−	−	+	+
10	+	−	+	+	−	+	−
11	+	+	−	−	−	+	+
12	+	−	−	−	−	+	+
14	+	+	−	−	−	+	−
17	+	+	−	−	−	+	+
19	+	+	−	−	+	+	+
21	+	−	−	−	−	+	+
22	+	+	−	−	+	+	+
24	+	+	−	−	−	+	+
27	+	−	−	−	−	+	+
28	+	+	+	−	−	+	+
30	+	+	+	−	+	+	+
Total + no	16	11	4	1	4	16	13

Abbreviations: [1]obstructive inflammation (+, positive; −, negative); [2]tumour boundary identification on PET images (+, influence; −, no influence); [3]abnormal density/signal at the site of pancreatic cancer on CT/MR (+, yes; −, no); [4]presence or absence of pancreatic duct dilation (+, presence; −, absence)

However, the results have no influence on tumour M staging, which is important for clinical management and outcomes.

Discussion

The present study was designed as a single-centre and prospective study. We compared the diagnostic and staging efficacy of ^{68} Ga-FAPI-04 PET/MR with ^{18}F-FDG PET/CT for pancreatic cancer.

Pancreatic cancer is characterised by vascular deficiency and plentiful desmoplastic stroma, accounting for 90% of the tumour volume. The stroma consists of extracellular matrix proteins and CAFs [21]. Our study revealed that the primary tumour could be visualised by ^{68} Ga-FAPI-04, which was consistent with previous studies [14, 16]. Fibrosis of the pancreas is often a striking feature of chronic pancreatitis [22]. ^{68} Ga-FAPI-04 was not more tumour-precise than ^{18}F-FDG and has a limitation of false-positive uptake caused by inflammation-induced fibrosis, which has been demonstrated by previous studies [16, 23]. In this study, there seemed to be an overlap of the uptake intensities in the pancreatic mass and obstructive pancreatitis of the pancreatic parenchyma, and it is crucial to differentiate pathological ^{68} Ga-FAPI-04 uptake from tumour-induced obstructive pancreatitis. The positive ^{68} Ga-FAPI-04 uptake caused by tumour-induced inflammation sometimes affects the visual interpretation of PET; thus, the qualitative reading of ^{68} Ga-FAPI-04 PET images sometimes must be combined with other radiological data.

Our results showed that ^{68} Ga-FAPI-04 might be better than ^{18}F-FDG in the assessment of lymph node metastasis in pancreatic cancer. This result was in accordance with previous research [24]. These findings may significantly impact clinical management. A recent study by Qin et al. proposed the contrary opinion. They found that the number of avid lymph nodes detected by ^{18}F-FDG was higher than that of ^{68} Ga-FAPI-04 in nasopharyngeal carcinoma (100 vs. 48) [25]. None of the lymph nodes was confirmed by histopathological results, but imaging follow-up was performed. Further studies with histopathological results are required.

We found that larger hepatic metastases usually had "ring-like" ^{68} Ga-FAPI-04 uptake at the edge of the lesion only. In many animal models, the highest tracer uptake is usually at specific tumour areas with a good blood supply [26]. Early studies showed that in the peritumoural hepatic parenchyma of hepatic metastases, the rate of sinusoidal hyperaemia was 95%, and the rate of fibrous proliferation was 58% [27]. However, the extent of CAF expression was consistent in peritumoural and intratumoural regions of liver metastases [28]. Thus, we speculate that the "ring-like" ^{68} Ga-FAPI-04 uptake in liver metastases might be related to sinusoidal congestion surrounding metastatic tumours.

^{18}F-FDG PET/CT, which has good accuracy, is a powerful screening tool for metastatic disease assessment. However, the assessment of liver lesions is inhibited by high

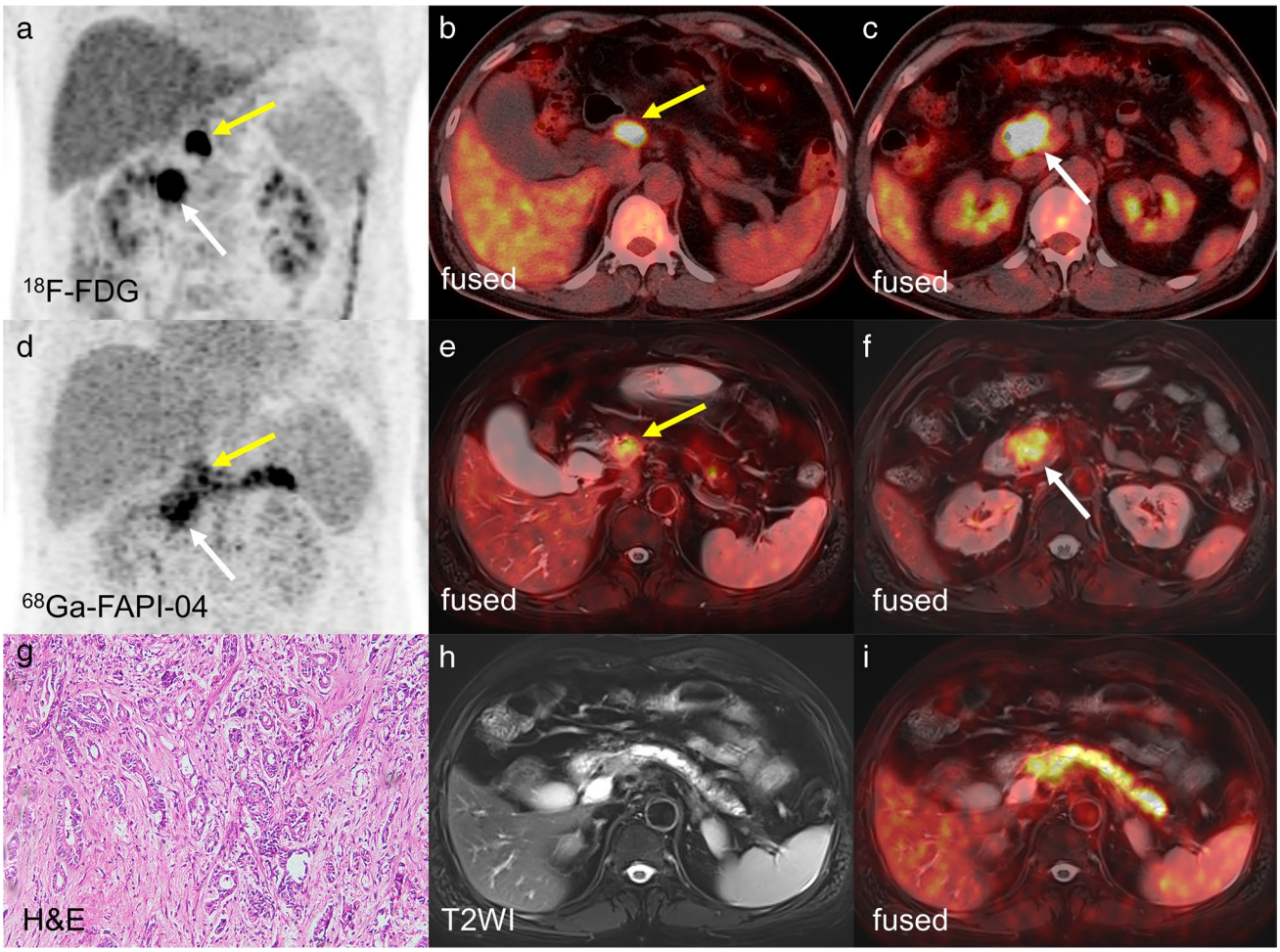

Fig. 2 A 53-year-old man (patient 24) with pancreatic ductal adenocarcinoma (PDAC). **a**–**f** ^{68} Ga-FAPI-04 PET/MR and ^{18}F-FDG PET/CT exhibited high focal uptake (FAPI: SUV_{max} = 9.59; FDG: SUV_{max} = 12.10) in the pancreatic head (white arrows) and lymph node metastasis (FAPI: SUV_{max} = 6.77; FDG: SUV_{max} = 15.40) in the lesser omentum (yellow arrows). **g** Haematoxylin–eosin (HE) staining of pancreatic cancer tissues (× 200 magnification). **h**, **i** Dilatation of the major pancreatic duct with obstructive pancreatitis-related ^{68} Ga-FAPI-04 uptake in the body and pancreatic tail (SUV_{max} = 11.70)

background liver uptake as well as other intrinsic technical limitations [29]. In contrast, ^{68} Ga-FAPI-04 demonstrates very low unspecific liver uptake and is expected to be superior for identifying liver metastasis. However, in five patients with liver metastasis in our cases, some ^{18}F-FDG hypermetabolic micrometastases were not detected by ^{68} Ga-FAPI-04, and the SUV_{max} was significantly lower in ^{68} Ga-FAPI-04 than in ^{18}F-FDG PET. This is contrary to previously published studies that showed that ^{68} Ga-FAPI-04 PET/CT identified more metastatic sites than ^{18}F-FDG with a significantly higher SUV [14, 24]. The reason for this discrepancy might be related to the difference in the origins of CAFs. Differences in progenitor cellular origins result in different phenotypes and functions of CAFs [30, 31]. Patients who were identified with pancreatic cancer as their only tumour or first primary tumour were included in this study, whereas the metastases reported in other studies consisted of mixed primary tumour compositions, with few pancreatic primary tumours.

As reported previously, pancreatic cancer may cause false-positive concentrations of ^{68} Ga-FAPI-04 in the inflammatory pancreatic parenchyma to some extent; therefore, we introduced PET/MR to explore the added value of MR [16]. Based on our results, obstructive inflammation of the pancreas might affect the interpretation of tumour foci in ^{68} Ga-FAPI-04 imaging, which is inferior to ^{18}F-FDG for the identification of liver metastases, and false-negative results would be expected for ^{68} Ga-FAPI-04 imaging in some metastatic lymph nodes. As mentioned above, MR provides more valuable information for its superior soft-tissue contrast and multiple sequence imaging to compensate for the deficiency of ^{68} Ga-FAPI-04 imaging [6, 17, 32]. Therefore, we think PET/MR may be a better partner for ^{68} Ga-FAPI-04 imaging of pancreatic tumours.

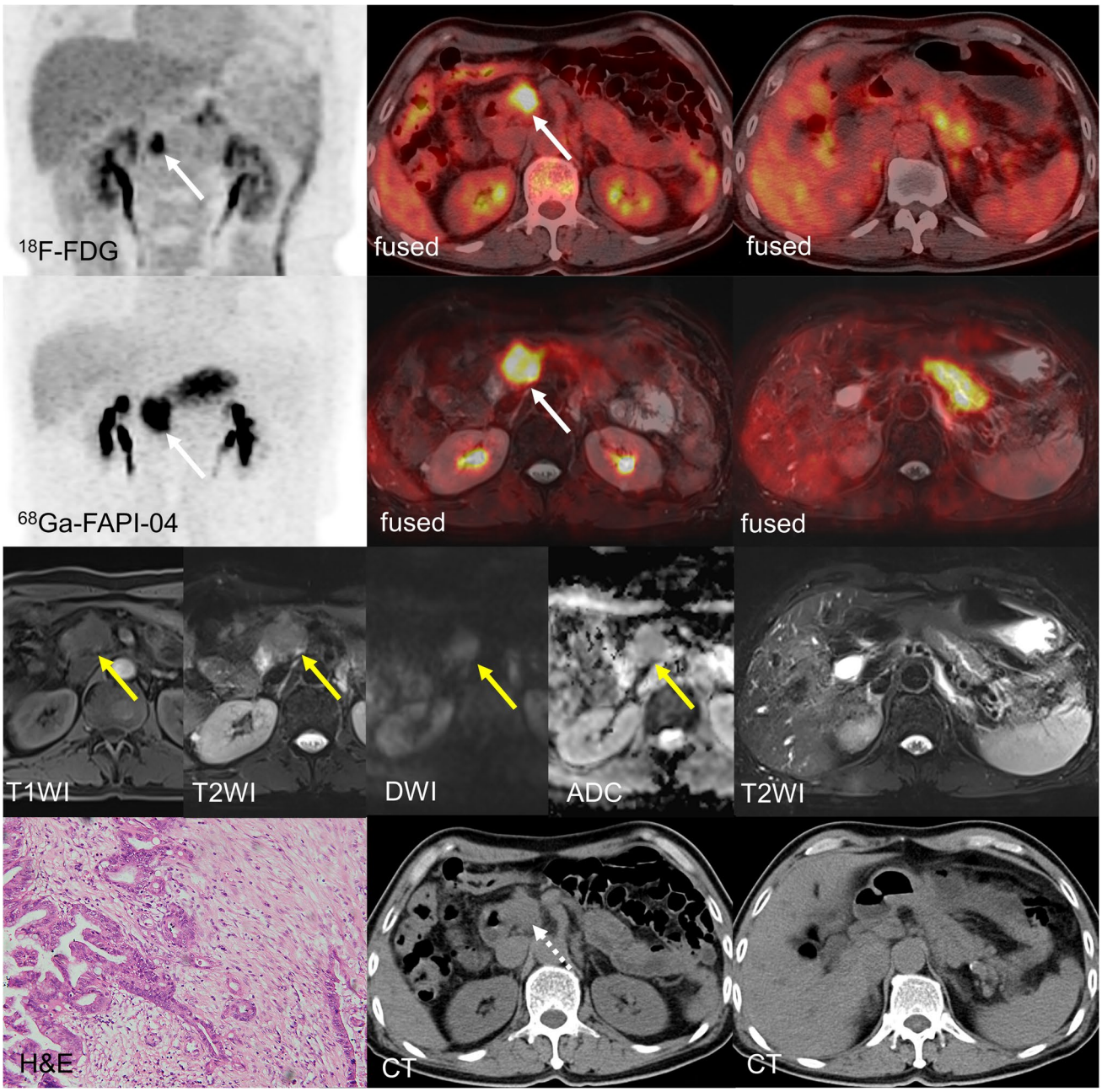

Fig. 3 A 72-year-old man (patient 17) with pancreatic ductal adenocarcinoma (PDAC). ^{68} Ga-FAPI-04 PET/MR and ^{18}F-FDG PET/CT exhibited high focal uptake (FAPI: $SUV_{max} = 19.30$; FDG: $SUV_{max} = 7.64$) in the pancreatic head (white arrows). Pancreatitis-related ^{68} Ga-FAPI-04 uptake could be seen in the pancreatic body and tail ($SUV_{max} = 14.9$), and nodular ^{18}F-FDG uptake could also be seen in the body of the pancreas ($SUV_{max} = 4.34$). On CT images, the pancreatic head lesion showed soft tissue density (dashed arrow), swelling of the pancreatic body and tail, and the main pancreatic duct appears ill defined, while MR images showed abnormal signal in the lesion (low signal on T1WI, slightly high signal on T2WI, high signal on DWI, and low signal on ADC, yellow arrows), accompanied by slight dilation of the main pancreatic duct, which enhanced the confidence of diagnosing pancreatic head carcinoma on ^{68} Ga-FAPI-04 images

The present study had several limitations. First, hardware differences between the two devices may lead to data heterogeneity; therefore, we normalised the two sets of data to ensure relative comparability. Second, histopathology results were not obtained for lymph node metastasis. Third, the present study was a single-centre based trial with a small sample size. Further studies with larger patient cohorts are needed to confirm these results.

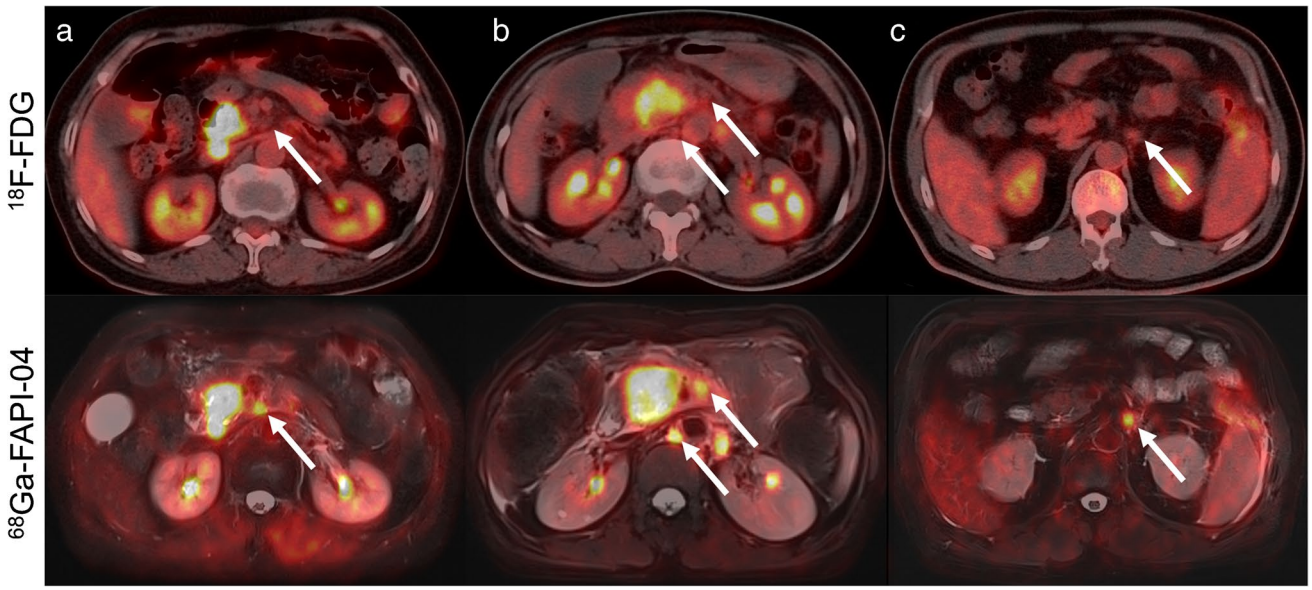

Fig. 4 In these three patients, ^{18}F-FDG-negative lymph nodes were ^{68} Ga-FAPI-04 positive (arrows)

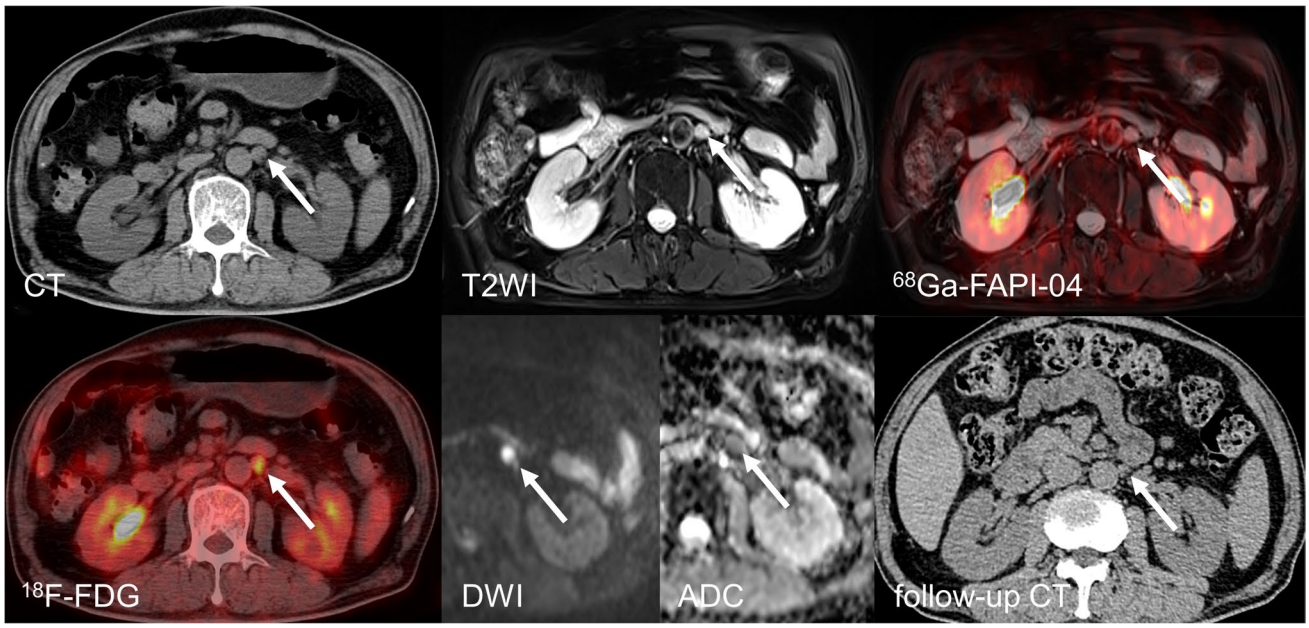

Fig. 5 Comparison of ^{18}F-FDG PET/CT and ^{68} Ga-FAPI-04 PET/MR of para-aortic lymph nodes in a 66-year-old man (patient 28). This lymph node measured 1.2 cm in short diameter and showed marked ^{18}F-FDG accumulation ($SUV_{max} = 5.6$). On ^{68} Ga-FAPI-04 PET/MR imaging, no increased radioactive uptake was seen in the enlarged node, which made it difficult to determine whether it was benign or malignant; however, MR signals showed significant changes (high signal on T2WI and DWI, low signal on ADC), which enhanced the confidence in diagnosing the metastatic lymph node. After chemotherapy, the lymph node was reduced to 0.7 cm on the follow-up CT images

Conclusion

In this prospective study, ^{68} Ga-FAPI-04 PET/MR demonstrated an equivalent detection rate to ^{18}F-FDG PET/CT for primary tumours of pancreatic cancer, and MR multiple sequence imaging of integrated PET/MR was helpful for explaining pancreatic lesions in patients with obstructive inflammation. ^{68} Ga-FAPI-04 PET might be better than ^{18}F-FDG PET in the detection of suspicious

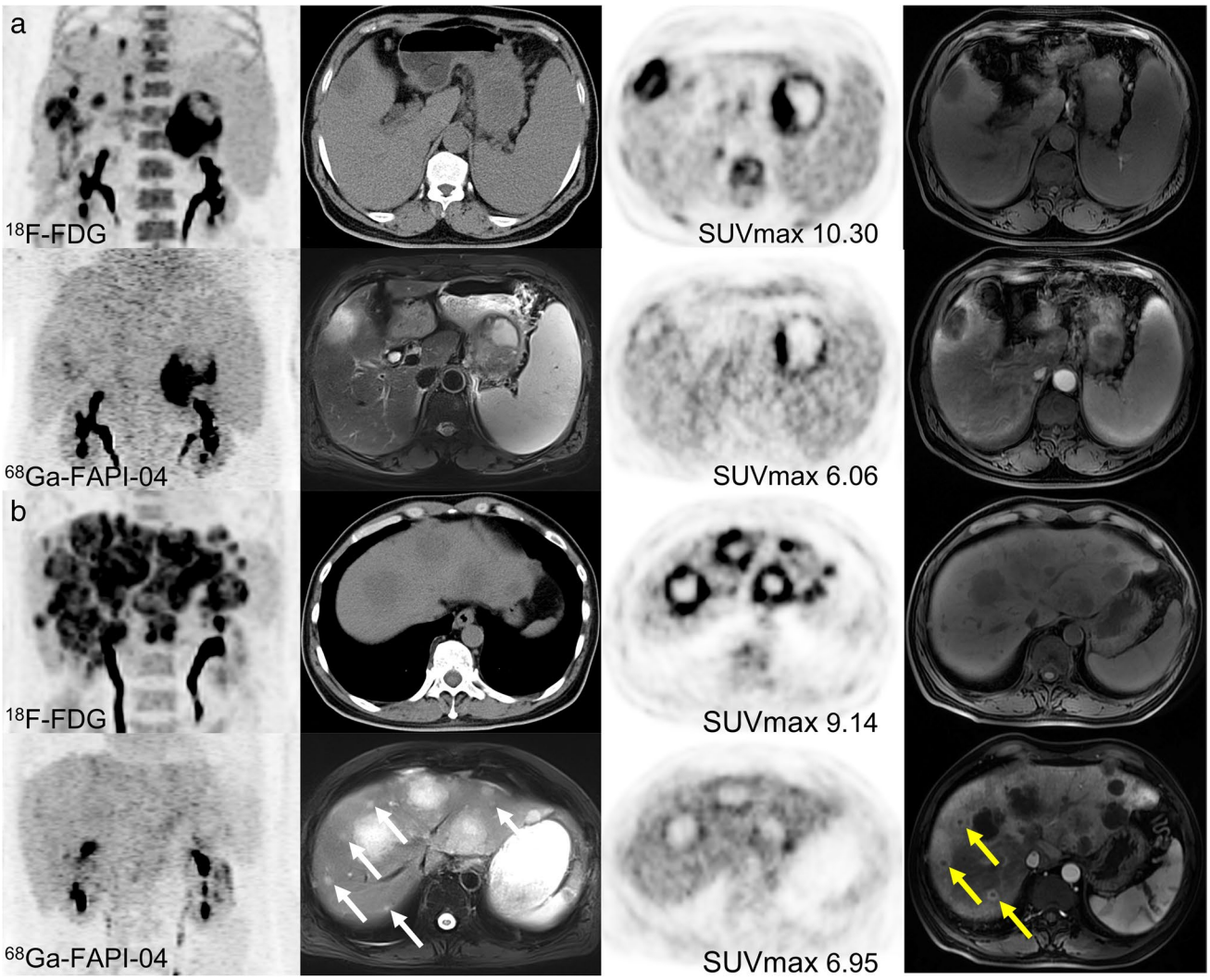

Fig. 6 In two liver metastatic patients with pancreatic tumours, ^{68} Ga-FAPI-04 uptake was detected at only the edge of liver metastases, and the ^{18}F-FDG uptake intensity was more obvious. All intrahepatic metastases with increased ^{18}F-FDG metabolism were detected by MRI, and more micrometastases undetectable by CT were identified by MRI (white arrows). These lesions showed typical ring enhancement in contrast-enhanced axial T1-weighted MR images (yellow arrows)

lymph node metastases, but the value of ^{68} Ga-FAPI-04 PET for N staging needs further study. The ^{68} Ga-FAPI-04 PET shows no obvious superiority over ^{18}F-FDG PET in detecting intrahepatic metastasis, but hybrid MR imaging was helpful in detecting the tiny metastatic foci.

Supplementary Information The online version contains supplementary material available at https://doi.org/10.1007/s00259-022-05729-5.

Author contribution Zeyu Zhang, Guorong Jia, Chao Cheng, and Changjing Zuo designed the study, interpreted the data, and led the writing and review of the manuscript. Kai Cao, Guixia Pan, Lu Zhang, and Tao Wang synthesised ^{68} Ga-FAPI-04 and performed the examination. Chao Cheng, Changjing Zuo, Zeyu Zhang, Guorong Jia, Qinqin Yang, Hongyu Meng, and Jian Yang collected clinical and imaging data. Chao Cheng and Changjing Zuo participated in the review of the manuscript.

Funding We gratefully acknowledge the financial support of the National Natural Science Foundation of China (Grant Nos. 82001867 and 81871390) and the "234 Discipline Climbing Plan" of the First Affiliated Hospital of Naval Medical University (Grant Nos. 2019YPT002 and 2020YPT002).

Availability of data and material Not applicable.

Code availability Not applicable.

Declarations

Ethics approval This article does not contain any studies with animals. All procedures of this study followed the principles of the Declaration of Helsinki. This prospective study was approved by the Ethics Committee of the First Affiliated Hospital of Naval Medical University (Changhai Hospital, CHEC2020-071).

Consent to participate All subjects provided written informed consent.

Consent for publication Informed consent was obtained from all individual participants included in this study.

Conflict of interest The authors declare no competing interests.

References

1. Siegel RL, Miller KD, Jemal A. Cancer statistics, 2020. CA Cancer J Clin. 2020;70:7–30. https://doi.org/10.3322/caac.21590.
2. Kleeff J, Korc M, Apte M, La Vecchia C, Johnson CD, Biankin AV, et al. Pancreatic cancer. Nat Rev Dis Primers. 2016;2:16022. https://doi.org/10.1038/nrdp.2016.22.
3. Kauhanen SP, Komar G, Seppänen MP, Dean KI, Minn HR, Kajander SA, et al. A prospective diagnostic accuracy study of 18F-fluorodeoxyglucose positron emission tomography/computed tomography, multidetector row computed tomography, and magnetic resonance imaging in primary diagnosis and staging of pancreatic cancer. Ann Surg. 2009;250:957–63. https://doi.org/10.1097/SLA.0b013e3181b2fafa.
4. Lee JW, O JH, Choi M, Choi JY. Impact of F-18 fluorodeoxyglucose PET/CT and PET/MRI on initial staging and changes in management of pancreatic ductal adenocarcinoma: a systemic review and meta-analysis. Diagnostics (Basel). 2020;10:952. https://doi.org/10.3390/diagnostics10110952.
5. Wang L, Dong P, Shen G, Hou S, Zhang Y, Liu X, et al. 18F-Fluorodeoxyglucose positron emission tomography predicts treatment efficacy and clinical outcome for patients with pancreatic carcinoma: a meta-analysis. Pancreas. 2019;48:996–1002. https://doi.org/10.1097/MPA.0000000000001375.
6. Rijkers AP, Valkema R, Duivenvoorden HJ, van Eijck CH. Usefulness of F-18-fluorodeoxyglucose positron emission tomography to confirm suspected pancreatic cancer: a meta-analysis. Eur J Surg Oncol. 2014;40:794–804. https://doi.org/10.1016/j.ejso.2014.03.016.
7. Erkan M, Hausmann S, Michalski CW, Fingerle AA, Dobritz M, Kleeff J, et al. The role of stroma in pancreatic cancer: diagnostic and therapeutic implications. Nat Rev Gastroenterol Hepatol. 2012;9:454–67. https://doi.org/10.1038/nrgastro.2012.115.
8. Nielsen MFB, Mortensen MB, Detlefsen S. Typing of pancreatic cancer-associated fibroblasts identifies different subpopulations. World J Gastroenterol. 2018;24:4663–78. https://doi.org/10.3748/wjg.v24.i41.4663.
9. Whittle MC, Hingorani SR. Fibroblasts in pancreatic ductal adenocarcinoma: biological mechanisms and therapeutic targets. Gastroenterology. 2019;156:2085–96. https://doi.org/10.1053/j.gastro.2018.12.044.
10. Piersma B, Hayward MK, Weaver VM. Fibrosis and cancer: a strained relationship. Biochim Biophys Acta Rev Cancer. 2020;1873:188356. https://doi.org/10.1016/j.bbcan.2020.188356.
11. von Ahrens D, Bhagat TD, Nagrath D, Maitra A, Verma A. The role of stromal cancer-associated fibroblasts in pancreatic cancer. J Hematol Oncol. 2017;10:76. https://doi.org/10.1186/s13045-017-0448-5.
12. Mikuła-Pietrasik J, Uruski P, Tykarski A, Książek K. The peritoneal "soil" for a cancerous "seed": a comprehensive review of the pathogenesis of intraperitoneal cancer metastases. Cell Mol Life Sci. 2018;75:509–25. https://doi.org/10.1007/s00018-017-2663-1.
13. Yang X, Lin Y, Shi Y, Li B, Liu W, Yin W, et al. FAP Promotes immunosuppression by cancer-associated fibroblasts in the tumor microenvironment via STAT3-CCL2 signaling. Cancer Res. 2016;76:4124–35. https://doi.org/10.1158/0008-5472.CAN-15-2973.
14. Kratochwil C, Flechsig P, Lindner T, Abderrahim L, Altmann A, Mier W, et al. 68Ga-FAPI PET/CT: tracer uptake in 28 different kinds of cancer. J Nucl Med. 2019;60:801–5. https://doi.org/10.2967/jnumed.119.227967.
15. Giesel FL, Kratochwil C, Lindner T, Marschalek MM, Loktev A, Lehnert W, et al. 68Ga-FAPI PET/CT: biodistribution and preliminary dosimetry estimate of 2 DOTA-containing FAP-targeting agents in patients with various cancers. J Nucl Med. 2019;60:386–92. https://doi.org/10.2967/jnumed.118.215913.
16. Röhrich M, Naumann P, Giesel FL, Choyke PL, Staudinger F, Wefers A, et al. Impact of 68Ga-FAPI PET/CT imaging on the therapeutic management of primary and recurrent pancreatic ductal adenocarcinomas. J Nucl Med. 2021;62:779–86. https://doi.org/10.2967/jnumed.120.253062.
17. Sagiyama K, Watanabe Y, Kamei R, Hong S, Kawanami S, Matsumoto Y, et al. Multiparametric voxel-based analyses of standardized uptake values and apparent diffusion coefficients of soft-tissue tumours with a positron emission tomography/magnetic resonance system: preliminary results. Eur Radiol. 2017;27:5024–33. https://doi.org/10.1007/s00330-017-4912-y.
18. Yeh R, Dercle L, Garg I, Wang ZJ, Hough DM, Goenka AH. The role of 18F-FDG PET/CT and PET/MRI in pancreatic ductal adenocarcinoma. Abdom Radiol (NY). 2018;43:415–34. https://doi.org/10.1007/s00261-017-1374-2.
19. Lindner T, Loktev A, Altmann A, Giesel F, Kratochwil C, Debus J, et al. Development of quinoline-based theranostic ligands for the targeting of fibroblast activation protein. J Nucl Med. 2018;59:1415–22. https://doi.org/10.2967/jnumed.118.210443.
20. Qin C, Shao F, Gai Y, Liu Q, Ruan W, Liu F, et al. 68Ga-DOTA-FAPI-04 PET/MR in the evaluation of gastric carcinomas: comparison with 18F-FDG PET/CT. J Nucl Med. 2022;63(1):81–8. https://doi.org/10.2967/jnumed.120.258467.
21. González-Borja I, Viúdez A, Goñi S, Santamaria E, Carrasco-García E, Pérez-Sanz J, et al. Omics approaches in pancreatic adenocarcinoma. Cancers (Basel). 2019;11:1052. https://doi.org/10.3390/cancers11081052.
22. Kleeff J, Whitcomb DC, Shimosegawa T, Esposito I, Lerch MM, Gress T, et al. Chronic pancreatitis. Nat Rev Dis Primers. 2017;3:17060. https://doi.org/10.1038/nrdp.2017.60
23. Luo Y, Pan Q, Yang H, Peng L, Zhang W, Li F. Fibroblast activation protein-targeted PET/CT with 68Ga-FAPI for imaging IgG4-related disease: comparison to 18F-FDG PET/CT. J Nucl Med. 2021;62:266–71. https://doi.org/10.2967/jnumed.120.244723.
24. Chen H, Pang Y, Wu J, Zhao L, Hao B, Wu J, et al. Comparison of [68Ga]Ga-DOTA-FAPI-04 and [18F] FDG PET/CT for the diagnosis of primary and metastatic lesions in patients with various types of cancer. Eur J Nucl Med Mol Imaging. 2020;47:1820–32. https://doi.org/10.1007/s00259-020-04769-z.
25. Qin C, Liu F, Huang J, Ruan W, Liu Q, Gai Y, et al. A head-to-head comparison of 68Ga-DOTA-FAPI-04 and 18F-FDG PET/MR in patients with nasopharyngeal carcinoma: a prospective study. Eur J Nucl Med Mol Imaging. 2021;48:3228–37. https://doi.org/10.1007/s00259-021-05255-w.
26. Loktev A, Lindner T, Burger EM, Altmann A, Giesel F, Kratochwil C, et al. Development of fibroblast activation protein-targeted radiotracers with improved tumor retention. J Nucl Med. 2019;60:1421–9. https://doi.org/10.2967/jnumed.118.224469.
27. Kanematsu M, Hoshi H, Yamada T, Nandate Y, Kato M, Yokoyama R, et al. Overestimating the size of hepatic malignancy on helical CT during arterial portography: equilibrium phase CT and pathology. J Comput Assist Tomogr. 1997;21:713–9. https://doi.org/10.1097/00004728-199709000-00006.
28. Peng J, Wang Y, Zhang R, Deng Y, Xiao B, Ou Q, et al. Immune cell infiltration in the microenvironment of liver oligometastasis

from colorectal cancer: intratumoural CD8/CD3 ratio is a valuable prognostic index for patients undergoing liver metastasectomy. Cancers (Basel). 2019;11:1922. https://doi.org/10.3390/cancers11121922.

29. Wang XY, Yang F, Jin C, Fu DL. Utility of PET/CT in diagnosis, staging, assessment of resectability and metabolic response of pancreatic cancer. World J Gastroenterol. 2014;20:15580–9. https://doi.org/10.3748/wjg.v20.i42.15580.
30. Sharon Y, Raz Y, Cohen N, Ben-Shmuel A, Schwartz H, Geiger T, et al. Tumor-derived osteopontin reprograms normal mammary fibroblasts to promote inflammation and tumor growth in breast cancer. Cancer Res. 2015;75:963–73. https://doi.org/10.1158/0008-5472.CAN-14-1990.
31. Neesse A, Bauer CA, Öhlund D, Lauth M, Buchholz M, Michl P, et al. Stromal biology and therapy in pancreatic cancer: ready for clinical translation? Gut. 2019;68:159–71. https://doi.org/10.1136/gutjnl-2018-316451.
32. Chen WS, Li JJ, Hong L, Xing ZB, Wang F, Li CQ. Comparison of MRI, CT and 18F-FDG PET/CT in the diagnosis of local and metastatic of nasopharyngeal carcinomas: an updated meta analysis of clinical studies. Am J Transl Res. 2016;8:4532–47.